Structure of the liquid–vapor interface of a metal from a simple model potential: Corresponding states of the alkali metals

ARTICLE *in* THE JOURNAL OF CHEMICAL PHYSICS · JULY 1998

Impact Factor: 2.95 · DOI: 10.1063/1.476615

3 AUTHORS:

Dmitriy Chekmarev
International Flavors & Fragrances Inc.
19 PUBLICATIONS **535** CITATIONS
SEE PROFILE

Meishan Zhao
University of Chicago
112 PUBLICATIONS **1,676** CITATIONS
SEE PROFILE

Stuart A. Rice
University of Chicago
717 PUBLICATIONS **22,553** CITATIONS
SEE PROFILE

Structure of the liquid–vapor interface of a metal from a simple model potential: Corresponding states of the alkali metals

Dmitriy Chekmarev, Meishan Zhao, and Stuart A. Rice
Department of Chemistry and The James Franck Institute, The University of Chicago, Chicago, Illinois 60637

(Received 6 February 1998; accepted 2 April 1998)

We present the results of self-consistent quantum Monte Carlo simulations of the structures of the liquid-vapor interfaces of alkali metals (Na, K, Rb, Cs) using a modified semiempirical empty-core model potential. The purpose of this investigation is to simplify the analysis of inhomogeneous metals sufficiently to permit qualitative inferences to be drawn about the properties of families of metals. Both electronic and ion density profiles along the normal to the surface show oscillations in the liquid–vapor transition zone. These oscillations closely resemble those found in previous simulation studies of the liquid–vapor interfaces of alkalis, based on sophisticated nonlocal model potentials. Because of its semianalytical representation, the model potential used in this paper allows considerable simplification in the computational scheme relative to the effort involved in the previously published simulations. We find liquid Na, K, Rb, and Cs to exhibit similar surface layering. Moreover, our results suggest the existence of a corresponding states representation of the properties of this class of metals. We expect this new analysis will be useful in predicting the qualitative properties of the surface structures of a broad range of pure liquid metals. © *1998 American Institute of Physics.* [S0021-9606(98)02526-4]

I. INTRODUCTION

Progress in developing a theoretical understanding of, say, the structure of a complex system, is often generated by combining the results of ''exact'' calculations with those from physically motivated approximate calculations. By ''exact'' calculations we mean complete analyses of very simple systems which, it is hoped, support the essential features of the structure of interest, or extended numerical calculations based on very complicated representations of the atomic interactions and motions in the particular system of interest. We identify as physically motivated approximate calculations those which strip from a theoretical description the contributions believed to be secondary, thereby simplifying the analysis sufficiently that broad generalizations concerning the similarities and differences in the structures of the members of a class of systems can be inferred. The complementary character of these types of theories plays an important role in our interpretation of experimental observations.

This paper is concerned with constructing a simplified description of the structure of the liquid–vapor interface of a metal, so that generalizations concerning the structure of that interface in classes of metals and alloys can be inferred; the approach described is intended to complement the more detailed theoretical description developed by Rice and co-workers.[1–14]

It is now well established, from the results of experimental studies[15–19] and from the results of self-consistent quantum Monte Carlo simulations, that the structure of the liquid–vapor interface of a typical simple metal is significantly different from that of a simple dielectric liquid. In the latter, the density profile along the normal through the interface (longitudinal density profile) is a smooth monotonic function falling from the density characteristic of the bulk liquid to effectively zero on the vapor side; near the triple point this falloff occurs over a range of about two to three molecular diameters. In the former, for temperatures close to the freezing point, the longitudinal density distribution in the interface exhibits stratification with a spacing of about one atomic diameter; the stratification extends for three to four atomic diameters on the bulk side of the interface. On the vapor side of the interface the longitudinal density distribution falls rapidly to zero, with a scale length of a fraction of an atomic diameter.

The difference between the structures of the liquid–vapor interfaces of simple metallic and nonmetallic liquids can be traced to the different forms of their potential energy functions. The potential energy of a Lennard-Jones fluid is rather accurately represented by a sum of density-independent pairwise interactions

$$H_{\mathrm{eff}}=\sum_{i<j} V(\mathbf{R}_i,\mathbf{R}_j), \tag{1}$$

whereas for a typical simple metal the potential part of the system Hamiltonian is given by

$$H_{\mathrm{eff}}=U_0[\rho_0(\mathbf{r}),n_{\mathrm{el}}(\mathbf{r})]+\sum_{i<j} V_{\mathrm{eff}}(\mathbf{R}_i,\mathbf{R}_j;n_{\mathrm{el}}(\mathbf{r})) \tag{2}$$

when a second-order pseudopotential perturbation theory representation is used.[2–9,20,21] In Eq. (2), U_0 is the ''structure-independent energy'' which does not depend explicitly on the positions of the ions, V_{eff} is the effective ion–ion interaction, $\rho_0(\mathbf{r})$ is the reference ion density distribution, and $n_{\mathrm{el}}(\mathbf{r})$ is the valence electron density distribution.

Although V_{eff} depends on the electron density, hence implicitly also on the ion density, it is the volume-dependent term U_0 which determines the characteristic features of the structure of the liquid metal–vapor interface.[2–14] In a homogeneous liquid metal this term, which determines the binding energy, is constant throughout the system.[20,21] In an inhomogeneous metallic system, such as the liquid–vapor interface, it is the variation of U_0 with density across the interface that leads to strong confinement of the ions, forcing them to stay in the region where the density is high. In this sense the electron density dependence of U_0, translated into a variation of U_0 with position in the interface, has an effect similar to that of a relatively steep wall. Accordingly, just as a liquid of hard spheres packed against a smooth hard wall is stratified in the region near the wall,[22] so also the longitudinal distribution of ions in the liquid–vapor interface of a metal is stratified.

The pseudopotential formalism,[23,24] in which the true interaction between atomic cores and conduction electrons is replaced by a weak effective interaction, has usually been executed at the level of second-order perturbation theory. When the representation of the pseudopotential accounts for the nonlocality inherent in the formalism, it has been very successful in reproducing the properties of crystalline and liquid metals.[20,23] All of the previously reported self-consistent quantum Monte Carlo simulation studies of the liquid–vapor interfaces of simple metals have used complex, nonlocal model potentials[2–14] [e.g., the optimized model potential (OMP),[25,26] the energy-independent model potential (EIMP),[27,28] etc.]. The results of these simulation studies agree very well with the available experimental data, but the use of a nonlocal pseudopotential engenders high computational cost because the nonlocality requires that a large number of the terms in the potential energy functional be computed iteratively many times during the course of the simulation. Of course, local model potentials are considerably easier to work with, but cannot be as realistic, and for some metals the nonlocal character of the pseudopotential is expected to be important. On the other hand, local model potentials are good choices for the calculation of the bulk properties of simple metals, especially when the broad, qualitative, aspects of the behavior of a group of metals are at the focus of interest.[20] Indeed, recent studies indicate that some local pseudopotentials are almost as good as their nonlocal counterparts at accounting for the crystal structures, the bulk binding energies, the lattice dynamics, and the elastic constants of many simple metals.[29]

The results of our previous self-consistent quantum Monte Carlo simulation studies[2–14] show that all the major features of the structure of the liquid–vapor transition zone of a metal are robust with respect to a range of changes in the pseudopotential employed in the simulations. We expect, then, that it should be possible to construct a theory of the properties of an inhomogeneous liquid metal using simple local pseudopotentials; this paper is concerned with the development of that theory. Using that local pseudopotential theory for self-consistent quantum Monte Carlo simulations of the structure of the liquid–vapor interfaces of simple metals enables us to study the surface structure of a broad class of metallic systems and to search for possible chemical trends with respect to the surface properties of the sp-bonded metals and their alloys.

We have chosen as a test system the family of alkali metals. These metals are simple enough that full nonlocal pseudopotential calculations can be carried out, and some of these calculations have been reported previously. We test self-consistent Monte Carlo simulations of the structure of the liquid–vapor interfaces of Na and Cs, carried out with our approximate local pseudopotential, against the corresponding simulations using nonlocal pseudopotentials.[8] Our results include calculations of the longitudinal singlet density distributions, both ionic and electronic, and the transverse ion pair correlations functions and structure factors from selected strata parallel to the planar surface. The latter, which reflect the in-plane structure of the system, determine (in the weak scattering limit) the relaxation time for the electrical conductivity parallel to the surface.[14] The overall transverse structure function in the liquid–vapor interface can be obtained experimentally using the technique of grazing incidence x-ray diffraction.[30]

As an example of the qualitative information obtainable from the results of calculations for a family of metals, we infer that the longitudinal density distributions in the liquid–vapor interfaces of the alkali metals provide evidence for a corresponding states representation of this class of metals. The possibility that a corresponding states representation of this class of metals exists is not at all obvious given the complexity of the contributions to the pseudopotential of any particular metal, and the differences between the pseudopotentials of the several metals in the family.

II. HAMILTONIAN OF INHOMOGENEOUS LIQUID METAL

To date, the only satisfactory theoretical description of the structure of the liquid metal–vapor interface is that provided by self-consistent quantum Monte Carlo simulations. Although a considerable effort has been made for 20 years (consult Ref. 31 for details), none of the available analytical models is capable of providing a satisfactory representation of a whole set of structural features found in the liquid–vapor interfaces of simple metals and their alloys. This situation is not surprising given the complexity of the analysis required for a quantitative representation of the properties of a mixture of electrons and ion cores, the inhomogeneous spatial distributions of which are not coincident in the liquid–vapor interface.

The analysis described in this paper is based on the density functional–pseudopotential theory of inhomogeneous metals developed by D'Evelyn and Rice[1–4] and later improved by Gryko and Rice[5–7] and Harris, Gryko, and Rice.[8,9] As in all pseudopotential theories, the strong direct interaction between the delocalized electrons and the ions is replaced by an effective nonlocal potential which accounts for the requirement that the states of the delocalized electrons are orthogonal to the states of the ion core electrons. The energy is then calculated as the sum of the zeroth-order energy associated with the immersion of a degenerate electron gas in a nonuniform continuum distribution of positive

charge (an inhomogeneous jellium), and the first- and second-order perturbation theory corrections for the interaction between the discrete ions and the electrons.[3] To second order in perturbation theory, the Hamiltonian of a liquid metal of N ions and NZ sp-valence electrons is then given by

$$\mathbf{H}=\sum_{i=1}^{N}\frac{\mathbf{p}_i^2}{2m}+U_0[\rho_0(\mathbf{r}),n_{\mathrm{el}}(\mathbf{r})]+\sum_{i<j}V_{\mathrm{eff}}(\mathbf{R}_i,\mathbf{R}_j;n_{\mathrm{el}}(\mathbf{r})), \tag{3}$$

where $\mathbf{p}_i$ is the momentum of the ith atom with mass m, $V_{\mathrm{eff}}(\mathbf{R}_i,\mathbf{R}_j;n_{\mathrm{el}}(\mathbf{r}))$ is the effective pair potential between ions i and j located at $\mathbf{R}_i$ and $\mathbf{R}_j$, respectively, and $\rho_0(\mathbf{r})$ and $n_{\mathrm{el}}(\mathbf{r})$ are the corresponding reference jellium and electron densities. The functional U_0 is a structure-independent contribution to the energy which is, however, dependent on the electron and jellium densities. To be consistent with the notation adopted in earlier work, in our discussion we use atomic units for length (1 a.u.$=0.529\,177$ Å) and energy (1 a.u.$=27.116$ eV). In some of the analysis described below we find it convenient to use the volume per atom, $\Omega=\rho^{-1}$.

A. Calculation of the effective pair potential

Instead of calculating the linear response function of the electron system in the inhomogeneous domain, we make a local density approximation (LDA) for the effective pair potential[3]

$$V_{\mathrm{eff}}(\mathbf{R}_i,\mathbf{R}_j;n_{\mathrm{el}})=V_H(|\mathbf{R}_i-\mathbf{R}_j|;\tfrac{1}{2}[n_{\mathrm{el}}(\mathbf{R}_i)+n_{\mathrm{el}}(\mathbf{R}_j)]), \tag{4}$$

with $V_H(R;n_{\mathrm{el}}^{\mathrm{LDA}})$ the interaction between two ions separated by $R=|\mathbf{R}_i-\mathbf{R}_j|$ in a homogeneous fluid with electron density $n_{\mathrm{el}}^{\mathrm{LDA}}$. This effective ion–ion interaction can be represented as a sum of three contributions,

$$V_H(R;n_{\mathrm{el}}^{\mathrm{LDA}})=\frac{Z^2}{R}-\frac{2Z^2}{\pi R}\int_0^\infty\frac{F_N(q)\sin(qR)}{q}\,dq+W_{\mathrm{corr}}(R). \tag{5}$$

The first term in Eq. (5) is the direct Coulomb repulsion between ions with valence Z. In many cases, especially for nonlocal pseudopotentials, the valence Z is replaced by the effective charge Z^*.[25–27] The second term in Eq. (5) is an indirect interaction, the so-called band structure energy, mediated by the conduction electrons; it lowers the energy of the system. Finally, $W_{\mathrm{corr}}(R)$ is the contribution to the energy arising from the Born–Mayer core–core repulsion[32] and the van der Waals core polarization interactions.[33,34] This contribution to the energy is usually small relative to the others even in the inhomogeneous domain (a detailed discussion concerning the effects associated with this term will be given later).

The calculation of the effective interatomic potential within the framework of second-order pseudopotential perturbation theory has become a standardized procedure (see, for example, Refs. 20 and 23, and references therein). One only has to specify the choice of the form for the pseudopotential and of the local-field function $G(q)$, which accounts for the exchange and correlation energies of the electrons; the latter is, essentially, a correction to the electron dielectric function calculated in the random-phase approximation (RPA). Provided the electron–ion pseudopotential is local, the so-called energy wave number characteristic $F(q)$ takes the simple form

$$F(q)=\frac{\Omega q^2}{8\pi}\left(\frac{1}{\epsilon(q)}-1\right)|\omega_{\mathrm{bare}}(q)|^2, \tag{6}$$

where $\omega_{\mathrm{bare}}(q)$ is the Fourier transform of the bare pseudopotential and $\epsilon(q)$ is the test-charge dielectric function[20] which, in turn, is given by

$$\epsilon(q)=1-\frac{1-\epsilon_h(q)}{1+[1-\epsilon_h(q)]G(q)}. \tag{7}$$

In Eq. (7), $\epsilon_h(q)$ is the dielectric function of the electron gas calculated in the Hartree approximation, i.e., with exchange and correlation neglected; $\epsilon_h(q)$ can be represented in the form

$$\epsilon_h(q)=1+\frac{4k_{\mathrm{F}}}{\pi q^2}\left(\frac{1}{2}+\frac{4k_{\mathrm{F}}^2-q^2}{8k_{\mathrm{F}}}\ln\left|\frac{2k_{\mathrm{F}}+q}{2k_{\mathrm{F}}-q}\right|\right), \tag{8}$$

where k_{F} denotes the Fermi wave number. In the free electron model, k_{F} is related to the electron density through $k_{\mathrm{F}}=(3\pi^2 n_{\mathrm{el}})^{1/3}$. Finally, we establish the connection between $F(q)$ and its normalized analog $F_N(q)$ in Eq. (5) by writing

$$F_N(q)=-\frac{q^2\Omega}{2\pi Z^2}F(q). \tag{9}$$

We note that when a nonlocal pseudopotential is used, the calculation of $F_N(q)$ and Z^* requires the self-consistent solution of a system of coupled nonlinear equations (see, for example, Ref. 27).

The calculation of $G(q)$ requires the solution of a many-body problem, for which several approximations have been proposed.[20] It has been observed that the calculated effective pair potentials are quite sensitive to the particular form of the local-field correction employed, especially for short distances, and that this sensitivity is more pronounced for polyvalent than for univalent simple metals. In our simulations of Na, K, and Rb we have used the function due to Vashishta and Singwi,[35] which satisfies the electron gas compressibility sum rule. Unfortunately, at the very low electron densities characteristic of liquid Cs the use of the Vashishta and Singwi function predicts an electron pair correlation function that becomes negative at small separations. To avoid this unphysical feature, for our simulations of Cs we used the Singwi–Sjolander–Tosi–Land (SSTL)[36] local-field factor, which does generate a realistic electron pair correlation function for this system.

The pseudopotential representation is not unique.[39] For any specified energy, there are many possible choices for a pseudopotential, ranging from parametrized local model potentials to nonlocal first-principles pseudopotentials. For the simulations reported in this paper we have used the empty-core model potential due to Ashcroft:[37]

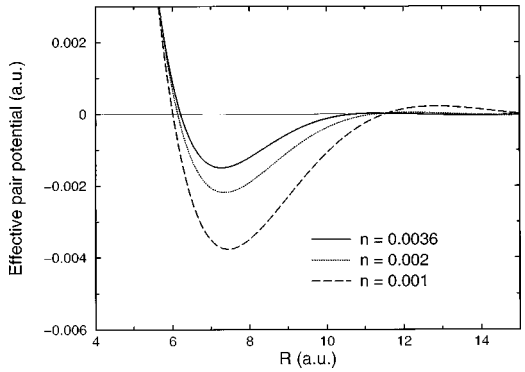

FIG. 1. Effective pair potential in liquid Na at several electron densities. Solid curve: $n=0.0036$ a.u.$^{-3}=0.02430$ atoms/Å^3. Dotted curve: $n=0.002$ a.u.$^{-3}=0.01350$ atoms/Å^3. Dashed curve: $n=0.001$ a.u.$^{-3}=0.00675$ atoms/Å^3.

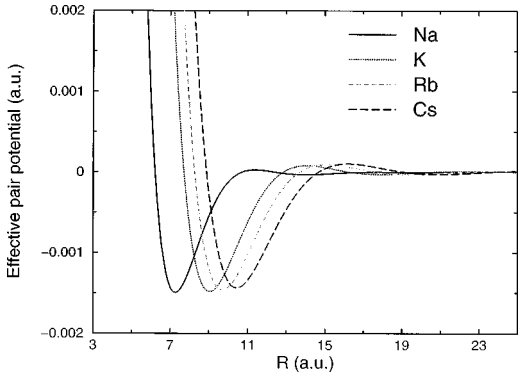

FIG. 2. Effective pair potentials in liquid alkali metals calculated at experimental bulk densities (see Ref. 56). Solid curve: Na. Dotted curve: K. Dashed curve: Rb. Long dashed curve: Cs.

$$\omega_{\text{bare}}(r)=0 \quad \text{for } r<R_c, \qquad \omega_{\text{bare}}(r)=-\frac{Z}{r} \quad \text{for } r>R_c, \tag{10}$$

where R_c is the empty-core radius, a single parameter that characterizes the atomic properties. Here R_c is typically adjusted to fit some experimental data;[23] the resulting values are usually found to be close to the accepted ionic radii. This simple local energy-independent model potential generates an effectively complete cancellation of the true potential in the region $r<R_c$.[23] Although only a rough approximation, the empty core potential is useful for description of the qualitative features of the electron–ion interaction in a metal. Indeed, it has been shown that this simple pseudopotential permits the development of a semiquantitative analysis of the trends in the structures of crystalline[38,39] and liquid metals.[39–41] The form factor associated with the empty-core model potential is

$$\omega_{\text{bare}}(q)=-\frac{4\pi Z}{\Omega q^2}\cos(R_c q), \tag{11}$$

and the corresponding energy wave number characteristic $F(q)$ has the analytic form

$$F(q)=\frac{2\pi Z^2}{\Omega q^2}\left(\frac{1}{\epsilon(q)}-1\right)\cos^2(R_c q). \tag{12}$$

For a system with given electron density and local-field function, the effective pair potential can then be easily calculated from Eqs. (4) and (5) via numerical integration.

For our calculations we used the following values for the empty-core radii of Na, K, Rb, and Cs: $R_c=1.70$ a.u., $R_c=2.20$ a.u., $R_c=2.45$ a.u., and $R_c=2.70$ a.u., respectively. These values are close to those reported by Evans and Schirmacher[42] who chose R_c so that the repulsive force part of the pairwise potential used in their calculations reproduces a realistic effective hard-sphere diameter for each alkali metal near its melting point [via the condition $S(0)=S_{\text{hs}}(0)$ when the packing fraction is 0.462, where $S_{\text{hs}}(q)$ is the static structure factor of the hard sphere fluid]. Figure 1 illustrates the density dependence of the effective pair interaction for liquid Na; the density dependences of the effective pair interactions in all simple metals are rather similar. The effective pair potentials for liquid Na, K, Rb, and Cs at their melting point densities are shown in Fig. 2. We have carried out Monte Carlo simulations of the bulk liquid phases of these metals with the potentials shown in Fig. 2 to obtain the bulk liquid pair correlation functions. The results of these calculations are displayed in Fig. 3, for the densities and temperatures described in the figure caption. Clearly, the agreement between the calculated and measured bulk liquid pair correlation functions is quite satisfactory.

B. Calculation of the structure-independent contribution

The sample used in all of our simulations is a slab of atoms with two free surfaces in the positive and negative z directions and periodic boundary conditions in the xy plane. The reference jellium distribution used is that introduced by Rice and co-workers;[5–8] it has the form

$$\rho(z,z_0,\beta)=\frac{\rho_{\text{bulk}}}{1+\exp((|z|-z_0)/\beta)}, \tag{13}$$

where z_0 is the position of the Gibbs dividing surface, β characterizes the width of the inhomogeneous region of the

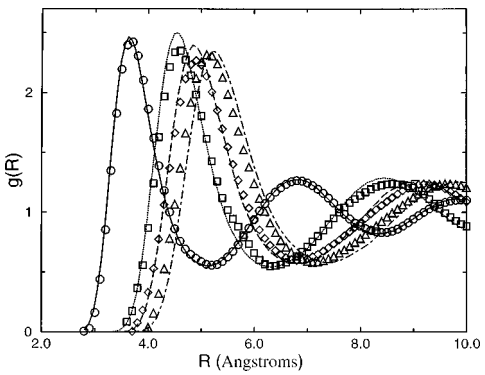

FIG. 3. Pair correlation functions of bulk liquid alkalis. Results of the bulk Monte Carlo simulations using the potentials of Fig. 2 (lines) and the experimental data of Ref. 56 (symbols). Liquid Na at 105 °C: calculated (———), experiment (∞∞). Liquid K at 70 °C: calculated (···), experiment (□□□). Liquid Rb at 100 °C: calculated (– – –), experiment (◇ ◇ ◇). Liquid Cs at 100 °C: calculated (–·–), experiment (△△△).

jellium profile, and $\rho_{\rm bulk}=N/2Az_0$, where N is a total number of atoms in the slab and A is a surface area of one free face of the slab. Given a reference profile of the form described by Eq. (13), the electronic density distribution can be obtained by solving the one-dimensional Kohn–Sham problem[43] equation

$$\left[-\frac{\hbar}{2m}\nabla_z^2+V_{\rm eff}(z)\right]\psi_N(z)=\varepsilon_N\psi_N(z), \tag{14}$$

with $V_{\rm eff}(z)$ an effective potential that includes the electron-positive background interaction along with the exchange-correlation potential. This equation was solved using the method introduced by Eguiluz *et al.*[44] The Kohn–Sham equation must be solved self-consistently because the eigenvector sought, $\psi_N(z)$, is used in the construction of $V_{\rm eff}(z)$.

The ''structure-independent'' energy U_0 is a function of the electron density $n_{\rm el}(\mathbf{r})$ and the positive (reference) charge density $\rho_0(\mathbf{r})$, but does not depend explicitly on the positions of ions. $U_0[\rho_0(\mathbf{r}),n_{\rm el}(\mathbf{r})]$, which is responsible for by far the largest contribution to the system energy (about 95%), can be represented as the sum of the kinetic energy, the electrostatic energy (which arises from the lack of coincidence of the electron and ion density distributions in the liquid–vapor transition zone), the exchange-correlation energy, and the electron–ion pseudopotential interaction,

$$U_0[\rho_0(\mathbf{r}),n_{\rm el}(\mathbf{r})]=E_{\rm kin}+E_{\rm es}+E_{\rm xc}+E_{\rm ps}. \tag{15}$$

The electronic kinetic energy $E_{\rm kin}$ can be calculated by using a local-density approximation with density gradient corrections[12] or by solving directly the self-consistent Kohn–Sham equation.[44] The electrostatic surface energy is given by

$$E_{\rm es}=2\pi A\int_0^\infty dz\int_0^\infty dz'[n_{\rm el}(z)n_{\rm el}(z')-\rho_0(z)\rho_0(z')]\times|z-z'|, \tag{16}$$

where $n_{\rm el}(z)$ is the longitudinal electron density distribution and $\rho_0(z)$ is the longitudinal ion density distribution. The exchange-correlation contribution $E_{\rm xc}$ was computed using the parametrization of Vosko, Wilk, and Nusair[45] for the local portion of the exchange-correlation energy, with density gradient corrections proposed by Langreth and Mehl.[46]

The last term in Eq. (15), the electron–ion pseudopotential contribution, must be discussed in more detail both because of the crucial role it plays in determining the structure of the liquid–vapor interface and because, unlike our previous calculations based on nonlocal pseudopotentials, the calculations described in this paper use a simple model local potential. This term can be written in the form

$$E_{\rm ps}=2A\int_0^\infty dz\ \rho_0(z)\epsilon_{\rm ps}[n_{\rm el}(z)], \tag{17}$$

where $\epsilon_{\rm ps}$ has the following form when a local pseudopotential is used:

$$\epsilon_{\rm ps}=3\int_0^1 f(\eta,\eta)\eta^2\,d\eta-\left[\frac{2\pi Z}{\Omega}\lim_{q\to0}\frac{1-F_N(q)}{q^2}+\frac{Z^2}{\pi}\int_0^\infty F_N(q)dq\right]+\left(\frac{C_1}{r_s}+\frac{C_2}{r_s^2}\right). \tag{18}$$

In Eq. (18), $r_s=((3/4\pi)n_{\rm el}^{-1})^{1/3}$ is the radius of a sphere containing one electron, $\eta=k/k_{\rm F}$, and $f(\eta,\eta)=Z\langle k|w_{nc}|k\rangle$ is the diagonal matrix element of the non-Coulombic part of the bare pseudopotential. The first term in Eq. (18) is the first-order correction to the system energy from the electron–ion pseudopotential. It is not influenced by screening since screening is merely a redistribution of the electron density (as long as the total charge is conserved) and, therefore, has no effect on average values. The next two terms (in square brackets) are second-order corrections. The last term represents empirical corrections to $\epsilon_{\rm ps}$ determined from the requirements that the bulk liquid have (effectively) zero vapor pressure and that the heat of vaporization at the experimental liquid density at 100 °C be correct. The inclusion of this correction term is found to be essential for reasons to be discussed shortly.

Thus far we have discussed only the calculation of the total system energy for a particular ionic configuration. In the systems of interest to us, specifically inhomogeneous liquid metals, ions are free to move, and thus the ionic configuration changes at each time step. As a result, a suitable average over all configurations accessible to the system must be carried out in order to determine the longitudinal and transverse density distributions in the liquid–vapor transition zone. The procedure used to obtain mutually self-consistent ion and electron density distributions is the following. For each ionic configuration $\{R_i\}$ we determine the reference continuum density $\rho_0(\mathbf{r})$. This jellium distribution is used to generate an electron density distribution via solution of the Kohn–Sham equation, the effective Hamiltonian given by Eq. (3) is calculated, and from it the energy of the system. A new configuration of the ion cores is generated by random displacements, and the procedure repeated. The new configuration of ion cores is accepted or rejected using the standard rules for a Monte Carlo simulation. The entire process is iterated until convergence of the system energy to a specified accuracy is attained.

III. DETAILS OF THE CALCULATIONS

We have carried out self-consistent quantum Monte Carlo simulations of liquid Na and K at 200 °C and of liquid Rb and Cs at 100 °C using the scheme due to Metropolis *et al.*[47] The dimensions of a slab containing 1000 ions were set initially to $L_0\times L_0\times 2L_0$ with periodic boundary conditions in the x and y directions and with free surfaces in the $\pm z$ directions (across the liquid–vapor transition zone). For convenience, periodic boundary conditions were also applied in the $\pm z$ directions, but at distances far from the Gibbs dividing surfaces. This convenience does not influence our results since it is found that only when the metallic character of the system is lifted by completely neglecting the structure-

independent contribution to the total energy is it possible for a few atoms to pass from the liquid (or the interface) to the gas phase.

The center of mass of the simulation sample was positioned at $z=0$, which is the location of the origin of the coordinates. The linear dimension of the simulation box, L_0, was chosen such that the initial density of the slab is equal to the known bulk density ρ_{bulk} at the temperature of interest. The simulation slab is about 16 layers deep (each roughly one atomic diameter in thickness), 8 layers for each half. Since the correlation length of the pair distribution function is only of order 3 atomic diameters, this slab is expected to be deep enough to guarantee that the liquid–vapor interface sits atop bulk liquid, an expectation that can be verified by computing the pair correlation function in the middle section of the simulation box and comparing it to that obtained from a simulation of the bulk liquid at the same density and temperature. We show later that our simulation slab meets this criterion.

The simulations were started by placing the particles at random positions within the boundaries of the slab. Initial configurations that have ion core-ion core overlaps are eliminated by a force-biased Monte Carlo simulation with periodic boundary conditions in all directions, using a scaled Lennard–Jones potential for the ion cores.

The trial configurations are generated by assigning a random displacement to each particle; ions are moved sequentially, one at a time. We define a simulation step unit, a *pass*, to be 1000 test moves with 1 move per particle. For each instantaneous ionic configuration thus produced the reference jellum parameters z_0 and β are determined using a weighted least-square fit of the discrete moments of the ion distribution to the continuous moments of $\rho(z,z_0,\beta)$ computed as described in Ref. 8. The minimization in this method was performed by means of the constrained quasi-Newton algorithm (NAG Fortran Library: subroutine E04JAF).

For each ionic configuration the corresponding electron density profile is a function of z, z_0, and β, and the structure-independent energy, U_0, is a function of the width parameter β and the liquid density ρ_{bulk}. To simplify the computational scheme we adopt the following approximate form for U_0:

$$U_0[\beta,\rho_{\mathrm{bulk}}]=Nu_0[\rho_{\mathrm{bulk}}]+2A\sigma[\beta,\rho_{\mathrm{bulk}}], \tag{19}$$

where $u_0[\rho_{\mathrm{bulk}}]$ is the structure-independent energy per particle of a homogeneous system with density ρ_{bulk}, and $\sigma[\beta,\rho_{\mathrm{bulk}}]$ is the surface energy (per unit area) of the reference jellium distribution represented by Eq. (13). Since for sufficiently large systems the fluctuations in ρ_{bulk} are usually negligibly small after the system has come to equilibrium, the first term in Eq. (19) remains virtually unchanged during the simulations and the second term is only weakly dependent on the bulk density. It is then reasonable to neglect the variation of the surface energy term with ρ_{bulk}. Thus, it is possible to tabulate the surface energies for one bulk density (e.g., the experimental density) as a function of β prior to the simulation run. In the course of the simulations u_0 is obtained from a polynomial expansion around the experimental bulk density and the surface energy term is found from a rational function interpolation using the table of the precomputed vales of σ vs. β.

The cutoff radius beyond which the pair potential is set to zero is taken, for each metal, to be slightly less than half (in the x and y directions) of the length of a side of the simulation box.[48] Of course, evaluation of the interaction energy for each pair of atoms for the millions of configurations produced during the course of a simulation is the most time-consuming procedure. Hence, it is far more advantageous to use a lookup table which is constructed once prior to a simulation run, and is accessed later in the course of the simulation whenever the values of $V_H(R;n_{\mathrm{el}})$ for a given separation and density are needed. We obtain the values for V_H from a cubic interpolation polynomial in Ω whose coefficients are in turn determined at a given R by linear interpolation from a table of coefficients that were computed in advance at 3000 equally spaced values of R^2. The coefficients in the latter are determined from the pair potentials calculated at four densities near the bulk experimental density by solving the pertinent Vandermonde matrix problem. The rest of the computational scheme for the effective ion–ion interactions is essentially the same as was described in our earlier work.[8]

Longitudinal density distributions are computed from a histogram of particle positions relative to the position of the center of mass of the slab. Profiles from both halves of the slab are averaged together to give the resultant longitudinal density distribution. Transverse density profiles for the bulk region of the slab are obtained using the same method.

To examine the in-plane structure of the model systems, we have computed transverse pair correlation functions and structure factors for thin sections sliced parallel to the interface. The pair correlation function is conventionally defined[48] by

$$g(R)=\frac{V}{N^2}\left\langle \sum_i \sum_{j\neq i} \delta(\mathbf{R}-\mathbf{R}_{ji}) \right\rangle, \tag{20}$$

where $\langle\cdots\rangle$ denotes an ensemble average. In practice, the delta function is replaced by a function which is nonzero in a small range of separations, and a histogram is compiled of all pair separations falling within each such range. When applied to the calculation of the pair correlation function in a thin slice parallel to the interface, Eq. (20) becomes

$$g(R)=\frac{2N(R,\Delta R)}{N_{\mathrm{slice}}^2}\left\langle \frac{V_{\mathrm{slice}}}{V_{\mathrm{int}}} \right\rangle, \tag{21}$$

where N_{slice} is the average number of particles within the section, V_{slice} is the total volume of the respective slice, $N(R,\Delta R)$ is the average number of pairs of particles within the section whose separations are larger than R but less than $R+\Delta R$, and V_{int} is the average volume of the intersection of the spherical shell with radius between R and $R+\Delta R$ and the thin slice. The in-plane structure factors can be obtained from $g(R)$ by numerical Fourier transform using the method introduced by Lado[49] (this method has the merit of preserving the orthogonality of the transform) or, alternatively, can be calculated directly by the algorithm of Kalos, Percus, and Rao.[50]

TABLE I. Summary of simulation characteristics.

System	T (K)	$\langle\rho_b\rangle$[a] (a.u.$^{-3}\times10^{-3}$)	ρ_b^{exp}[b] (a.u.$^{-3}\times10^{-3}$)	σ^e[c] (a.u.)	P_a[d] (%)	N_R[e] (millions)	N_{st}[f] (millions)
Na	473	3.50	3.59	6.60	37	19.0	8.0
K	473	1.83	1.89	8.18	47	18.8	8.0
Rb	373	1.49	1.51	8.76	46	18.8	8.0
Cs	373	1.24	1.20	9.31	57	31.0	8.0

[a]$\langle\rho_b\rangle$ is the average density of the simulation slab, in a.u.$^{-3}\times10^{-3}$.
[b]ρ_b^{exp} is the experimental bulk density of the liquid metal (Ref. 56), in a.u.$^{-3}\times10^{-3}$.
[c]σ is the effective ionic diameter ($1/\langle\rho_b\rangle=\sigma^3$), in a.u.
[d]P_a is the percentage of moves accepted by the Metropolis algorithm.
[e]N_R is the number of initial configurations rejected, in millions.
[f]N_{st} is the number of configurations used in collecting statistics, in millions.

The calculations we report have been carried out for about 30 000 (40 000 for liquid Cs) Monte Carlo passes for each alkali metal. For each metal, the last 8000 passes were used to obtain the final statistics. In Table I we list some of the parameters pertinent to each of the simulations.

All of the simulations reported in this study were carried out on SGI Power Challenge L and SGI Power Challenge XL parallel computers.

IV. RESULTS AND DISCUSSION

We have evaluated the structure-independent energy per atom, $u_0(\rho)$, using the model potential described in the preceding sections, including the density corrections, $C_1/r_s+C_2/r_s^2$, which were parametrized to reproduce the observed bulk density, heat of vaporization, and (zero) vapor pressure at 100 °C. Figure 4 displays, as one example, the corrected and uncorrected functions $u_0(\rho)$ for Na; the behavior of $u_0(\rho)$ for the other alkali metals is similar. We note that, in contrast to the results obtained using the EIMP nonlocal pseudopotential,[8] the correction term for the local pseudopotential adopted in this paper is quite large, and increases in importance as the atomic number of the alkali metal increases. For example, the correction term for the local pseudopotential contributes 12%–14% of the system binding energy (compared to only 3% for the EIMP model of liquid Cs) at densities near the experimental bulk liquid density of the alkali metals, and varies slowly as the density decreases in the interface.

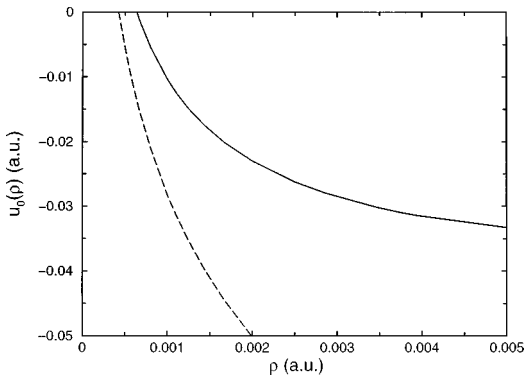

FIG. 4. Structure-independent energy per atom for Na: uncorrected (– – –), with empirical corrections (———).

Of course, the large magnitude of the contribution to the energy from the empirical correction to the empty core local pseudopotential is an indicator that said model potential cannot, alone, within the framework of second-order pseudopotential perturbation theory, generate a realistic description of an inhomogeneous liquid metal. Given the very strong density dependence of the uncorrected form of $u_0(\rho)$, it is not surprising that simulations of the structure of the liquid–vapor interface of Cs using it show that, although the system remains liquid, the ion density distribution is stratified across the whole slab, with the oscillations of the three outermost layers of the liquid–vapor interface substantially enhanced. Moreover, the average ionic density in the central portion of the slab is higher than that of bulk liquid Cs. Despite being rather impractical, this oversimplified model gives a picture which is qualitatively consistent (i.e., with well-pronounced surface layering) with the results produced by far more thorough nonlocal models. The corrections to $u_0(\rho)$ do seem to adequately compensate for the failings of the empty core pseudopotential, so that it provides a good description of both the structure and equation of state of the bulk liquid metal and of the binding energies of solid (BCC) Na and Cs at $T=0$ K. Including the contributions to the energy arising from polarization and the Born–Mayer repulsion we find $E_{\text{tot}}=-0.2288$ a.u. (experimental value:[51] -0.2297 a.u.) and $E_{\text{tot}}=-0.1720$ a.u. (experimental value:[51] -0.1726 a.u.) for Na and Cs, respectively.

That the density dependence of the structure-independent energy is the source of the unique structure of the liquid–vapor interface of a metal was first demonstrated in the work of D'Evelyn and Rice[3] and Harris, Gryko, and Rice.[8] We have carried out simulations of the liquid–vapor interface of Cs with the term U_0 omitted from the Hamiltonian, and the Cs pair potential computed for a bulk liquid atomic volume of $\Omega=850$ a.u. (Cs exp: $\Omega=830.16$ a.u.). The longitudinal density profile in the liquid–vapor interface of this pseudodielectric model system is displayed in Fig. 5, which should be compared with the longitudinal density distribution displayed in Fig. 6 of Ref. 8. The results reported in this paper reproduce all of the major qualitative features reported by Harris, Gryko, and Rice. In particular, the longitudinal density distribution associated with the pseudodielectric model system is much wider than that predicted when U_0 is retained in the system Hamiltonian, and it obvi-

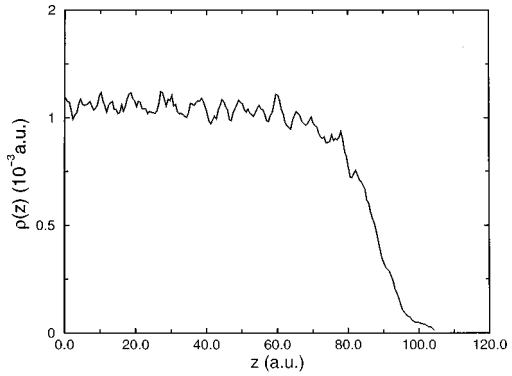

FIG. 5. Longitudinal density profile of liquid Cs without the structure-independent contribution U_0 at 100 °C.

ously lacks the stratification characteristic of realistic liquid metal–vapor interfaces systems.

The structure-independent energies per atom of liquid Na and liquid Cs, computed from the corrected empty core local pseudopotential model and from the EIMP nonlocal pseudopotential model,[27,28] are compared in Fig. 6; the agreement between these energies is satisfactory. Accordingly, we expect the density distributions computed for systems with these pseudopotentials to be nearly the same; the validity of this expectation is demonstrated in Figs. 7 and 8. In Fig. 7, we show the longitudinal density distribution in the liquid–vapor interface of Na computed using the corrected empty core pseudopotential; this is to be compared with the distribution shown in Fig. 4 of Ref. 8, which was computed using the EIMP nonlocal pseudopotential. A similar comparison is shown in Fig. 8 for the longitudinal density distribution in the liquid–vapor interface of Cs (see Table I). Given that the melting point of Na is 97.8 °C, we cannot exclude the possibility that a simulation carried out at 100 °C will not correspond to the stable liquid because of the limited accuracy of the pseudopotential. For that reason we have carried out simulations of the liquid–vapor interface of Na at 200 °C.

Despite the differences between the local empty core and EIMP pseudopotentials, the predicted longitudinal density distributions are nearly the same. In both cases the stratification extends for about three atomic diameters into the bulk liquid, with a spacing equal to the effective atomic diameter. That the stratification is not an artifact due to the finite size of the simulation box can be seen by computing the transverse ion density profile which is uniform but noisy, with a noise amplitude considerably smaller than the amplitudes of the peaks in the longitudinal density distribution. Also, the transverse structure factors calculated by the method of Kalos, Percus, and Rao[50] for thin slabs parallel to the liquid–vapor interface reveal no structure peculiar to crystalline ordering, confirming that the interface is isotropic in the xy plane.

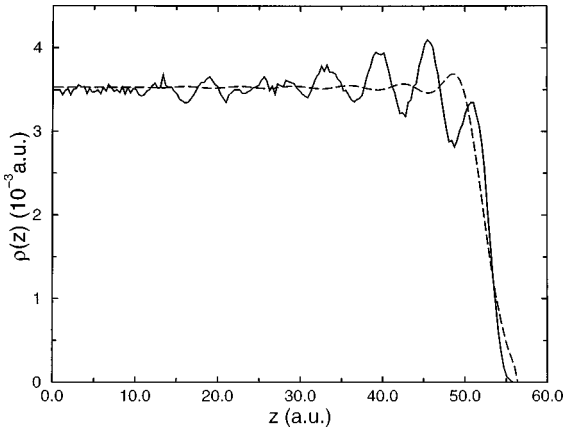

FIG. 7. Ionic (———) and electronic (– – –) surface density profiles normal to the Na liquid–vapor interface at 200 °C.

As to the electron density distribution, for both pseudopotential models the outermost peak in the longitudinal valence electron density distribution lies close to the position of the minimum between the first two peaks in the longitudinal ion core density profile. We have previously interpreted this displacement to be a consequence of the competition between minimization of the Coulomb energy, which is achieved when there is coincidence of the electron and ion core distributions, and the increase in the kinetic energy of the valence electrons associated with a gradient in the electron density. We expect this feature of the longitudinal valence electron and ion core distributions to be generic in

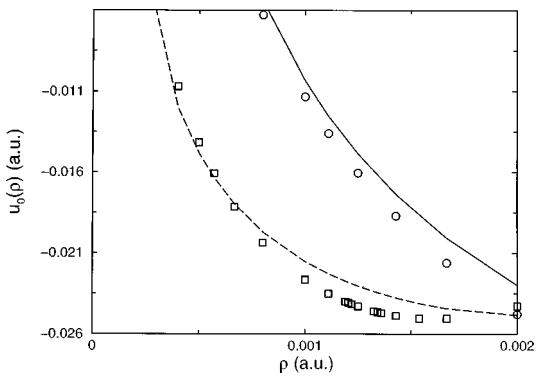

FIG. 6. Structure-independent energy per atom for Na calculated using the local pseudopotential model (———) and the EIMP model (Refs. 27 and 28) (∘∘∘). Structure-independent energy per atom for Cs calculated using the local pseudopotential model (– – –) and the EIMP model (□□□).

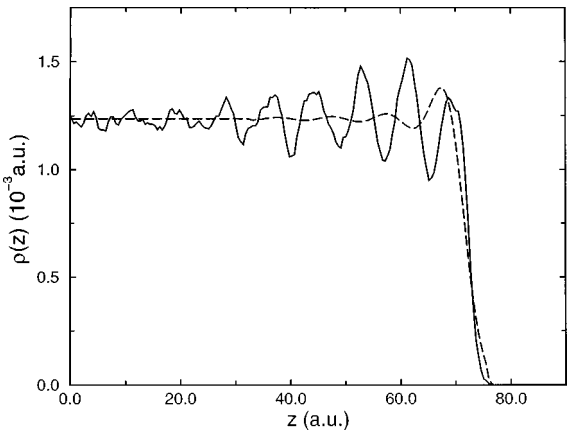

FIG. 8. Ionic (———) and electronic (– – –) surface density profiles normal to the Cs liquid–vapor interface at 100 °C.

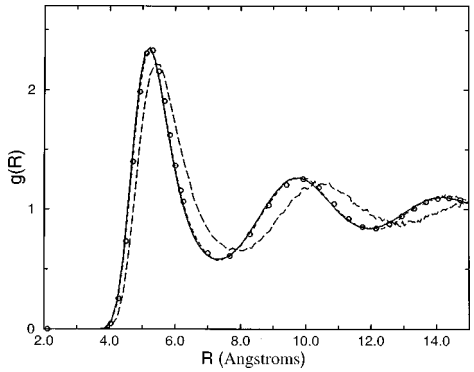

FIG. 9. Transverse correlation functions for selected layers from the Cs slab. Bulk region (———), second peak (---), first or outermost peak (– – –). The pair correlation function (∞) obtained from the bulk Monte Carlo simulation at the density corresponding to the inner stratum of the interface (only a representative set of points is shown).

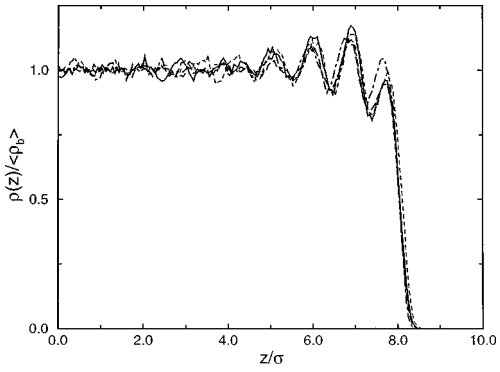

FIG. 10. Normalized longitudinal ion density profiles for liquid Na (———) at 200 °C, liquid K (---) at 200 °C, liquid Rb (– – –) at 100 °C, and liquid Cs (– – –) at 100 °C. The scaling length σ is an effective atomic diameter (consult Table I for details).

simple liquid metals.[8,12] Although we have emphasized the great similarity between the structures of systems with local and nonlocal pseudopotentials, there remain small differences between the fine structure found in the longitudinal density profiles of those systems, e.g., the magnitudes of the maxima and minima of the density and their absolute positions.

We have also examined how the stratification of the liquid–vapor interface affects the in-plane structure of the liquid. Our results qualitatively support those reported earlier by Harris, Gryko, and Rice[8] for the liquid–vapor interfaces of Na and Cs. In particular, in Fig. 9 we display the transverse pair correlation functions of Cs, computed for the outermost stratum and the next-to-outermost stratum of the interface. As the observation point moves across the interface from the liquid to the vapor side, notwithstanding passage through swings of the local density of $\pm 25\%$, there is very little change in the pair correlation function, noting the small shift outward in the positions of the second and third peaks. This insensitivity of the transverse pair correlation function to the point local density is successfully accounted for by the Fischer–Methfessel[52,53] extended local density approximation. In contrast to the results obtained by of Harris, Gryko, and Rice,[8] the local empty core pseudopotential model does not produce a statistically significant increase in the amplitude of the first peak of the transverse pair correlation function taken from a slice through a peak in the longitudinal ion density profile relative to that in the bulk liquid.

We have also carried out self-consistent quantum Monte Carlo simulations of the liquid–vapor interfaces of K (at 200 °C) and Rb using the corrected empty core pseudopotential. Figure 10 displays the longitudinal ion density distributions in the liquid–vapor interfaces of Na, K, Rb, and Cs, expressed in terms of the reduced variables $\rho(z)/\langle\rho_b\rangle$ and z/σ with $\sigma=\langle\rho_b\rangle^{-1/3}$. Within the statistical error of our results (relative standard deviation of the outermost peak amplitude=7%), these longitudinal density distributions are identical. Put in different words, our results show that there exists an approximate ''*law of corresponding states*'' for the structures of the liquid–vapor interfaces of alkali metals.

The existence of a law of corresponding states for the structures of the liquid–vapor interfaces of a family of metals is not at all obvious. For the case of simple liquids, the law of corresponding states is a consequence of pair interactions which depend only on a strength parameter ϵ and a range parameter σ through the functional form $V(R)=\epsilon f(R/\sigma)$. There is no reason to believe that, given the differences in electron density and core interactions, a potential of that form can be written for each of the members of a family of liquid metals. Nevertheless, it appears to be the case that for liquid metals the part of the effective pair potential which has the most influence in determining the bulk structure is the soft core (the part that typically does not exceed k_BT). As can be seen from the calculations displayed in Fig. 2, the soft core contributions to the total effective pair potential look virtually alike for all the metals considered in this work. Egelstaff *et al.*[54] proposed that the only parameter combination which determines the structure of a liquid metal is $r\rho^{1/3}$, which is viewed as a natural consequence of the density dependence of k_F. This notion has been thoroughly reexamined and confirmed in the subsequent work of Hayter *et al.*[55] We display in Fig. 11, in reduced variables, the bulk pair correlation functions computed for our simple models of Na, K, Rb, and Cs; the results show that the bulk pair correlation functions also support the existence of corresponding states of these liquids. However, Hayter *et al.*[55] also found

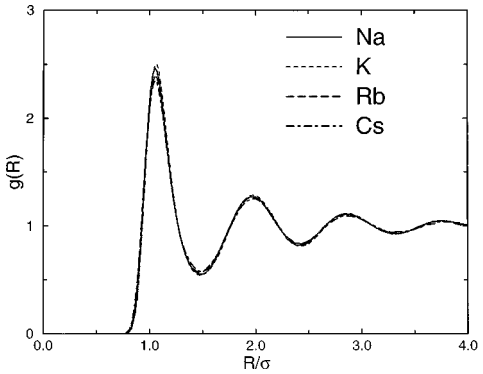

FIG. 11. Bulk pair correlation functions of liquid Na (———), liquid *K* (---), liquid Rb (– – –), and liquid Cs (– – –) plotted using the scaled position variable (see text for discussion). Temperatures and densities are the same as in Fig. 3.

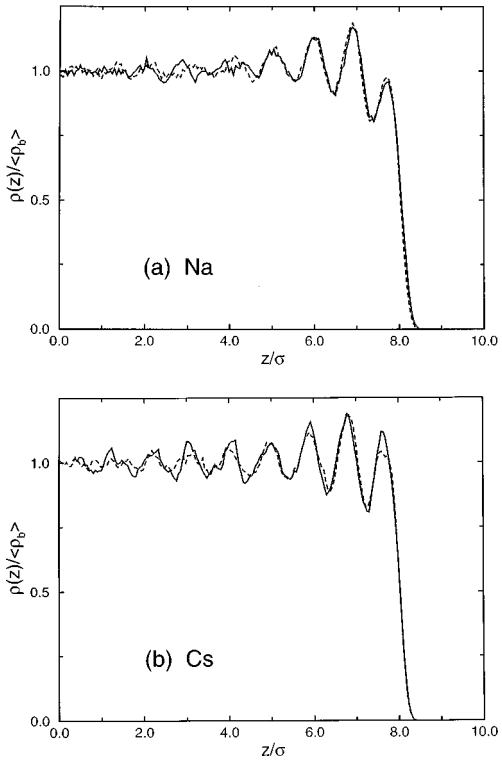

FIG. 12. Normalized surface transition zone density profiles for liquid Na (a) and Cs (b). Full potential model (———) and the simplified model (---) with the term W_{corr} omitted.

that at a more detailed level, uniform scaling of the properties of a family of metals may fail, especially for heavy alkalis, because of a contribution most likely arising from the screening which introduces a physical length that need not scale as $\rho^{-1/3}$. Although our interfacial transverse density distributions agree within the statistical error of the simulations, there does appear to be a difference between that for Cs and those for Na, K, and Rb, which might be a signature of the breakdown of the scaling which underlies the definition of corresponding states.

To the extent that only qualitative features of the structure of the liquid–vapor interface are sought, the model pseudopotential can be further simplified. We show in Fig. 12 the longitudinal ion density distributions in the liquid–vapor interfaces of Na and Cs computed using instead of the full empty core pseudopotential model one generated by neglecting $W_{\mathrm{corr}}(R)$. The most notable difference between these distributions is in the height of the outermost peak of Cs, which for the system with the simplified potential model is slightly smaller in amplitude; the rest of the structure in the density distribution is unchanged within the statistical error of the simulations. And, as shown, the omission of $W_{\mathrm{corr}}(R)$ has even less effect on the transition zone density distribution of Na.

One of the most important arguments in favor of the use of a local model potential such as described in this paper is computational convenience. We estimate that the calculation scheme reported in this paper is threefold faster than the Harris–Gryko–Rice computational scheme which uses a nonlocal pseudopotential. The increase in computational speed arises from the semianalytical representation of the local pseudopotential and the use of more efficient computational algorithms. This speed enhancement will be of great value when simulations are undertaken of the liquid–vapor interfaces of polyvalent metals and their alloys; for these complex metals computational schemes based on nonlocal pseudopotentials suffer from extremely slow convergence.[10,12]

ACKNOWLEDGMENTS

We thank Dr. J. Harris and Dr. A. Gomez for kindly providing part of the program codes. This work has been supported by a grant from the National Science Foundation.

[1] M. P. D'Evelyn and S. A. Rice, Phys. Rev. Lett. **47**, 1844 (1981).
[2] M. P. D'Evelyn and S. A. Rice, J. Chem. Phys. **78**, 5081 (1983).
[3] M. P. D'Evelyn and S. A. Rice, J. Chem. Phys. **78**, 5225 (1983).
[4] M. P. D'Evelyn and S. A. Rice, Discuss. Faraday Soc. **16**, 71 (1982).
[5] J. Gryko and S. A. Rice, J. Phys. F **12**, L245 (1982).
[6] J. Gryko and S. A. Rice, J. Non-Cryst. Solids **61–62**, 703 (1984).
[7] J. Gryko and S. A. Rice, J. Chem. Phys. **80**, 6314 (1984).
[8] J. G. Harris, J. Gryko, and S. A. Rice, J. Chem. Phys. **87**, 3069 (1987).
[9] J. G. Harris, J. Gryko, and S. A. Rice, J. Stat. Phys. **48**, 1109 (1987).
[10] A. Gomez and S. A. Rice, J. Chem. Phys. **101**, 8094 (1994).
[11] S. A. Rice, J. Non-Cryst. Solids **205–207**, 755 (1996).
[12] M. Zhao, D. Chekmarev, Z. Cai, and S. A. Rice, Phys. Rev. E **56**, 7033 (1997).
[13] M. Zhao, D. Chekmarev, and S. A. Rice, J. Chem. Phys. **108**, 5055 (1998).
[14] S. A. Rice, J. Gryko, and U. Mohanty, ''Structure and Properties of the Liquid-Vapor Interface of a Simple Metal,'' in *Fluid Interfacial Phenomena*, edited by C. A. Croxton (Wiley, New York, 1986).
[15] L. Bosio and M. Oumezine, J. Chem. Phys. **80**, 6318 (1984).
[16] O. M. Magnussen, B. M. Ocko, M. J. Regan, L. E. Berman, P. S. Pershan, and M. Deutsch, Phys. Rev. Lett. **74**, 4444 (1995).
[17] M. J. Regan, E. H. Kawamoto, S. Lee, P. S. Pershan, N. Maskil, M. Deutsch, O. M. Magnussen, B. M. Ocko, and K. Penanen, Phys. Rev. Lett. **75**, 2498 (1995).
[18] M. J. Regan, O. M. Magnussen, E. H. Kawamoto, P. S. Pershan, B. M. Ocko, N. Maskil, M. Deutsch, S. Lee, K. Penanen, and L. E. Berman, J. Non-Cryst. Solids **205–207**, 762 (1996).
[19] M. J. Regan, H. C. Tostmann, P. S. Pershan, O. M. Magnussen, E. DiMasi, B. M. Ocko, and M. Deutsch, Phys. Rev. B **55**, 10 786 (1997).
[20] J. Hafner, *From Hamiltonian to Phase Diagrams* (Springer-Verlag, Berlin, 1987).
[21] N. W. Ashcroft, and D. Stroud, in *Solid State Physics*, edited by F. Seitz H. Ehrenreich, and D. Turnbull (Academic, New York, 1978), Vol. 33.
[22] J. S. Rowlinson and B. Widom, *Molecular Theory of Capillarity* (Clarendon, Oxford, 1982).
[23] V. Heine and D. Weaire, in *Solid State Physics*, edited by F. Seitz, H. Ehrenreich, and D. Turnbull (Academic, New York, 1970), Vol. 24.
[24] W. A. Harrison, *Pseudopotentials in the Theory of Metals* (Benjamin, New York, 1966).
[25] R. W. Shaw, Jr., Phys. Rev. **174**, 769 (1968).
[26] R. W. Shaw, Jr., J. Phys. C **2**, 2335 (1969).
[27] C. H. Woo, S. Wang, and M. Matsuura, J. Phys. F **5**, 1836 (1975).
[28] M. Matsuura, C. H. Woo, and S. Wang, J. Phys. F **5**, 1849 (1975).
[29] L. Pollack, J. P. Perdew, J. He, M. Marques, F. Nogueira, and C. Fiolhais, Phys. Rev. B **55**, 15 544 (1997).
[30] B. N. Thomas, S. W. Barton, F. Novak, and S. A. Rice, J. Chem. Phys. **86**, 1036 (1987).
[31] A. Gomez and E. Chacon, Phys. Rev. B **46**, 723 (1992).
[32] T. L. Gilbert, J. Chem. Phys. **49**, 2640 (1968).
[33] J. J. Rehr, E. Zaremba, and W. Kohn, Phys. Rev. B **12**, 2062 (1975).
[34] J. C. Upadhyaya, S. Wang, and R. A. Moore, Can. J. Phys. **58**, 905 (1980).
[35] P. Vashishta and K. S. Singwi, Phys. Rev. B **6**, 875 (1972).
[36] K. S. Singwi, A. Sjolander, M. P. Tosi, and R. H. Land, Phys. Rev. B **1**, 1044 (1970).
[37] N. W. Ashcroft, Phys. Lett. **23**, 48 (1966).
[38] J. Hafner and V. Heine, J. Phys. F **13**, 2479 (1983).

[39] J. Hafner, in *Cohesion and Structures*, edited by D. G. Pettifor and F. R. de Boer (North–Holland, Amsterdam, 1989), Vol. 2.
[40] J. Hafner and G. Kahl, J. Phys. F **14**, 2259 (1984).
[41] J. Bocker, Z. Gurskii, and K. Heinzinger, J. Phys. Chem. **100**, 14 969 (1996).
[42] R. Evans and W. Schirmacher, J. Phys. C **11**, 2437 (1978).
[43] W. Kohn and L. J. Sham, Phys. Rev. A **140**, 1133 (1965).
[44] A. G. Eguiluz, D. A. Campbell, A. A. Maradudin, and R. F. Wallis, Phys. Rev. B **30**, 5449 (1984).
[45] S. H. Vosko, L. Wilk, and M. Nusair, Can. J. Phys. **58**, 1200 (1980).
[46] D. C. Langreth and M. J. Mehl, Phys. Rev. B **8**, 1809 (1983).
[47] N. Metropolis, A. W. Rosenbluth, M. N. Rosenbluth, A. H. Teller, and E. Teller, J. Chem. Phys. **21**, 1087 (1953).
[48] M. P. Allen and D. J. Tildesley, *Computer Simulation of Liquids* (Clarendon, Oxford, 1989).
[49] F. Lado, J. Comput. Phys. **8**, 417 (1971).
[50] M. H. Kalos, J. K. Percus, and M. Rao, J. Stat. Phys. **17**, 111 (1977).
[51] R. Hultgren, P. D. Desai, D. T. Hawkins, M. Gleiser, K. K. Kelly, and D. D. Wagman, *Selected Values of the Thermodynamic Properties of the Elements* (ASM Metals Park, OH, 1973).
[52] J. G. Harris and S. A. Rice, J. Chem. Phys. **86**, 5731 (1987).
[53] J. Fisher and M. Methfessel, Phys. Rev. A **22**, 2836 (1980).
[54] P. A. Egelstaff, D. I. Page, and C. R. T. Heard, J. Phys. C **4**, 1453 (1971).
[55] J. B. Hayter, R. Pynn, and J.-B. Suck, J. Phys. F **13**, L1–L6 (1983).
[56] Y. Waseda, *The Structure of Non-Crystalline Materials-Liquids and Amorphous Solids* (McGraw–Hill, New York, 1980).